The 9th European Congress on Computational Methods in Applied Sciences and Engineering
ECCOMAS Congress 2024
3 – 7 June 2024, Lisboa, Portugal

A 3D PARTICLE MODEL FOR REINFORCED CONCRETE FRACTURE ANALYSIS

N. MONTEIRO AZEVEDO[*1], M.L. BRAGA FARINHA[*2] AND S. OLIVEIRA[*3]

[*]Concrete Dams Department
Laboratório Nacional de Engenharia Civil (LNEC)
Av. do Brasil 101, 1700-066 Lisboa, Portugal
e-mail: [1]nazevedo@lnec.pt, [2]lbraga@lnec.pt, [3]soliveira@lnec.pt, www.lnec.pt/barragens-betao

Key words: Reinforced concrete, Discrete element, Reinforcement Model, Fracture.

Summary. A numerical model for the analysis of reinforced concrete structures must incorporate tools capable of representing the formation and propagation of cracks, their effect on the overall behavior of the structure, and the interaction between reinforcement and concrete. Detailed rigid particle models (PM) that take directly into consideration the physical mechanisms and the influence of the material aggregate structure have gained relevance and have shown to be able to predict, evaluate and understand cracking phenomena in concrete. The 3D particle models correlate well with experimental results from concrete specimens, particularly in terms of elastic response, peak values, fracture process and fracture location. This paper presents the 3D explicit formulation of steel reinforcement bars using discrete elements with cylindrical geometry. The incorporation of steel elements allows the particle model to be applied to the analysis of fracture in reinforced concrete structures. The rigid elements of cylindrical geometry interact with the concrete, modeled by spherical particles, through a contact interface. The model is validated in three-point beam bending tests, without transverse steel reinforcement. The numerical results obtained show that the proposed model correctly simulates the actual behavior, representing the fracture evolution process and the load-displacement relationship for different steel ratios.

1 INTRODUCTION

It is possible to predict, evaluate and understand cracking phenomena in quasi-brittle materials through numerical models, among them detailed rigid particle models (PM) have emerged. PMs by taking directly into consideration the material grain structure and the granular physical interaction mechanisms can reproduce complex crack patterns and macroscopic behaviours, similar to those observed in laboratory tests, in rock [1, 2], concrete [3-5], reinforced concrete [6, 7], old masonry [8, 9] and asphalt mixtures [10, 11]. PM models are conceptually simpler than models based on a continuous approach and, since they are based on an idealized discontinuous medium, the development of failure surfaces and their interaction occurs naturally.

To evaluate reinforced concrete structures, a numerical model must include tools that can accurately represent crack formation and propagation, and their effect on the structure's overall behaviour. To model reinforced concrete structures with a PM, it is necessary to consider the

model for the steel reinforcement and consider steel/concrete interaction mechanisms. In the context of the continuum-based finite element method (FEM), there are three different approaches to represent reinforcement bars, depending on the type of problem being analysed [12]: i) discrete representation, ii) distributed representation and iii) embedded representation. In similar mesoscale models based either in the Rigid-Body-Spring Model (RBSM) or in the Lattice Discrete Particle Model, steel reinforcement bars can be represented by 1D bar elements, Euler or Timoshenko beams, that interact with the concrete particles via a spring interface [13-16]. In the RBSM a finer particle discretization of the steel reinforcement has also been adopted [17, 18]. When a finer particle discretization is followed, different material properties are adopted for the particles representing the reinforcement bars, and the steel/concrete interface is handled as a usual particle/particle interaction.

In 3D DEM based PMs, the most straightforward way to include the reinforcement is to discretize the reinforcement bars using lines of sphere particles of diameter equal to the bar diameter [7], but this may lead to a higher number of particles to be adopted given the particle size. This paper presents a 3D explicit formulation of reinforcement bars using discrete elements with cylindrical geometry, based on the 2D model proposed in [7] for concrete, that has also been applied in old masonry strengthening analysis [19]. The incorporation of steel elements allows the particle model to be applied to the analysis of fracture in reinforced concrete structures. The model is validated in three-point beam bending tests without transverse steel reinforcement. As shown here, there is a good correlation between the PM reinforced model and the experimental results, in terms of the load/displacement relationship and the fracture process for various levels of reinforcement.

2 PARTICE MODEL (PM)

2.1 Voronoi-generalized contact model (VGCM-3D)

In this work, a 3D Voronoi-generalized contact model (VGCM-3D) [20, 21] is adopted. In the VGCM-3D model, the contact surface and the contact point location are defined by the Voronoi tessellation of the spherical particles gravity centers, Figure 1. The common Voronoi facet is the contact surface and the vertexes of the Voronoi facet including the gravity centre of the Voronoi facet are considered to be the local contact points locations, Figure 1.

By incorporating the VGCM-3D contact model, the PM model takes into account the polyhedral shaped particles in an approximate way, but still keeps the simplicity of spherical particle models and does not require a significant increase in the computational effort. Given the normal ($k_n^{[J]}$) and shear stiffness ($k_s^{[J]}$) of each local contact point, the normal and shear forces increments are obtained following an incremental linear law:

$$\Delta F_{\square}^{[J,N]} = -k_n^{[J]} \Delta x_{\square}^{[J,N]} = -k_n^{[J]} \left(\dot{x}_i^{[J]} \Delta t \right) n_i \tag{1}$$

$$\Delta F_i^{[J,S]} = -k_s^{[J]} \Delta x_i^{[J,S]} = -k_s^{[J]} \left(\dot{x}_i^{[J]} \Delta t \right) - \Delta x_{\square}^{[J,N]} n_i \tag{2}$$

where $\Delta x_{\square}^{[J,N]}$ is the contact displacement normal increment stored as a scalar, $\Delta x_i^{[J,S]}$ is the contact shear displacement increment stored as a vector and n_i is the contact unit normal.

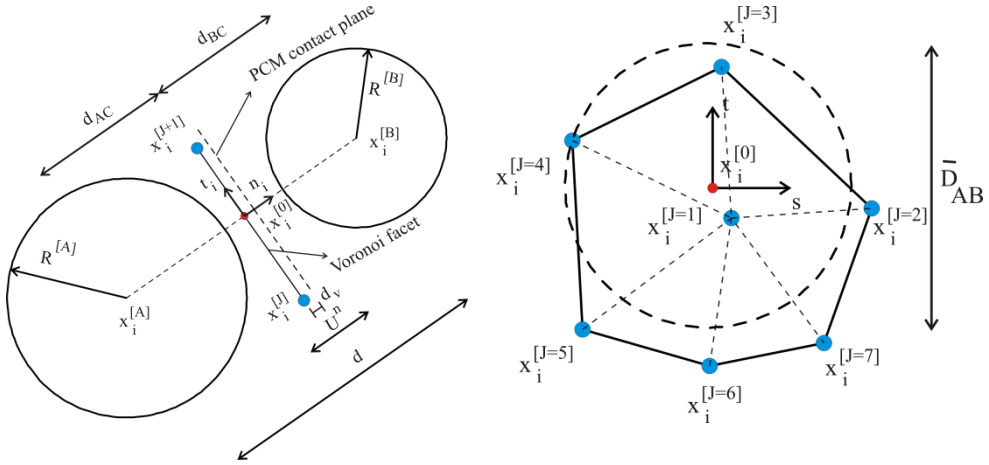

Figure 1: VGCM-3D contact model with variable number of local points given by the Voronoi facet vertexes and its gravity centre

2.2 Local contact stiffness and local contact strength

The VGCM-3D contact stiffness is defined based on the Young's modulus of the equivalent continuum material ($\bar{E}$) and on a constant that relates the normal and the shear stiffness spring value (α):

$$k_n^{[J]} = \frac{\bar{E}}{d} A_c^{[J]} \tag{3}$$

$$k_s^{[J]} = \alpha \, k_n^{[J]} \tag{4}$$

where, $A_c^{[J]}$ is the contact area associated with the local point j and d is the distance between the particles centre of gravity. The contact strength properties are defined based on the maximum contact tensile stress ($\sigma_{n.t}$)), the maximum contact cohesion stress (τ) and the local contact point area:

$$F_{n.max}^{[J]} = \sigma_{n.t} \, A_c^{[J]} \tag{5}$$

$$C_{max}^{[J]} = \tau \, A_c^{[J]} \tag{6}$$

2.3 PM Generation

Figure 2 shows the adopted PM generation procedure for the uniaxial tests that are used for calibration proposed in Section 3. An aggregate quantity of 568.5 kg/m^3 comprising particle dimensions ranging from 8.0 to12.0 mm in diameter was considered in the PMs. The particles representing the mortar are subsequently introduced adopting a porosity value of 0.1 and a uniform distribution, featuring diameters ranging between 8.0 and 9.0 mm.

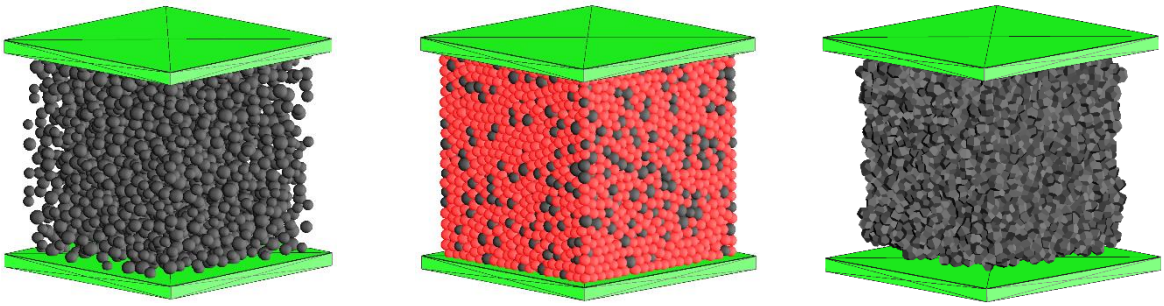

a) aggregate particle insertion: particles with 8.0 to 12.0 mm diameter (black)

b) compact assembly with particles with 8.0 to 9.0 mm diameter representing the mortar (red)

c) Laguerre–Voronoi cells of the aggregate particles with 8.0 to 9.0 mm diameter.

Figure 2: PM generation steps for concrete.

3.4 Vectorial bilinear weakening model (BL)

A bilinear softening damage model, Figure 3, can be adopted for the contact in the normal and shear directions [2, 3, 4]. Given the current total contact damage the maximum values of tensile and cohesive strength are reduced accordingly. The contact damage is given in an approximate way by the sum of tensile and shear damage. In each direction, the damage value is defined as a function of the maximum contact displacement in that direction. The BL contact model can be used with confidence in PM fracture studies with the following advantages in detailed 3D PM DEM-based models: a reduced number of contact strength parameters requiring calibration and lower associated computational costs [21].

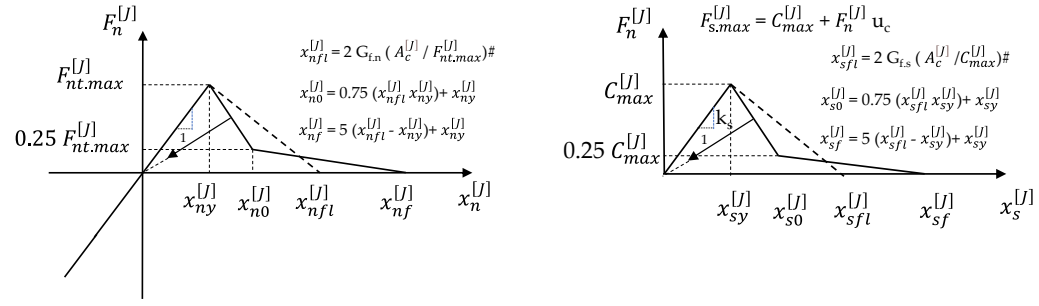

a) Normal direction

b) Shear direction

Figure 3: Bilinear softening under tension and shear contact constitutive model

2.5 Reinforcement model

A given steel reinforcement is modeled using several rigid cylinders that interact with each other at the connection nodes. In this model, the elastic and strength properties are concentrated in the connection zones. Figure 4 shows the interaction model between two rigid cylinders at a given interaction node.

As in the MP model, each rigid cylinder has six degrees of freedom. It should be noted that the lumping of elastic and strength properties at the interaction node simplifies the

establishment of non-linear constitutive models (axial, shear, bending and torsion) when compared to equivalent FEM-based formulations. The laws of interaction at the point of connection between the cylindrical elements representing the reinforcement bar follow the principles defined for the Parallel Bond contact model [1], with the exception of how to calculate the location of the interaction node and the definition of the axial direction at the same point, defined below. A similar reinforcement model that adopts spherical particles with a given inter-particle distance and a cylindrical cover has been proposed for 3D DEM based PMs [22].

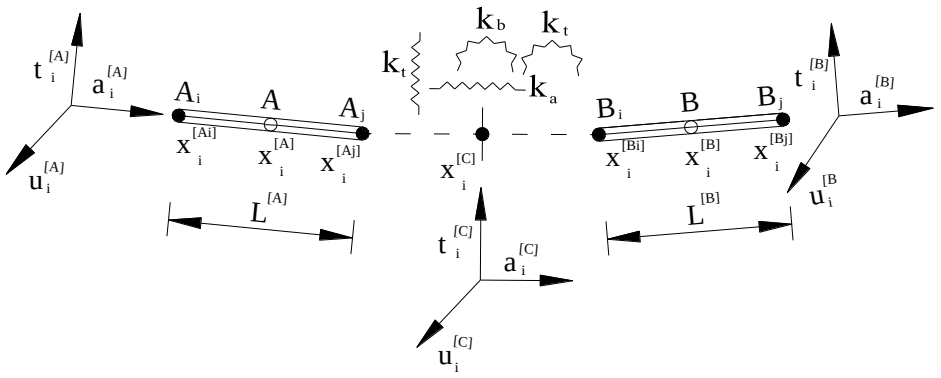

Figure 4: Steel bar model - Lumped properties at the interaction node.

The location of the interaction node, $x_c^{[C]}$, where the elastic and strength properties are concentrated, is given by the average of the coordinates of the end nodes of each rigid cylinder adopted in the discretization of the steel element:

$$x_c^{[C]} = 0.5\left(x_i^{[AJ]} + x_i^{[BI]]}\right) \tag{7}$$

where $x_i^{[AJ]}$ is the location of the center of gravity of the final end of rigid cylinder A, and $x_i^{[BI]}$is the location of the center of gravity of the initial end of rigid cylinder B. Both the final and initial locations are obtained in each calculation step from the member's center of gravity, its length and the axial direction. In each calculation step, the axial direction of the connection node is given by the average of the axial directions of the rigid members under analysis:

$$a_i^{[C]} = 0.5\left(a_i^{[A]} + a_i^{[B]}\right) \tag{8}$$

The stiffness values adopted for a given connection zone of a steel beam are given by:

$$k_a^{\square} = \frac{EA}{L};\ k_t^{\square} = \frac{GI}{L};\ k_b^{\square} = \frac{EI}{L};\ k_\theta^{\square} = \frac{EJ}{L} \tag{9}$$

where $k_a^{\square}$ and $k_t^{\square}$ are, respectively, the axial and shear stiffness of the connection node, $k_b^{\square}$ and $k_\theta^{\square}$ are, respectively, the bending and torsional stiffness of the connection node, L = ($L^{[A]}$ + $L^{[B]}$) / 2.0 is the length associated with the connection node given as a function of the neighboring cylindrical elements, $A = \frac{\pi D^2}{4}$ is the cross-sectional area of the steel beam and D

is the bar diameter, $I = \frac{\pi D^4}{64}$ is the moment of inertia of the cross-section, $J = \frac{\pi D^4}{32}$ is the polar moment of inertia of the cross-section of a circular section of diameter D, E is the Young's modulus of the steel beam and G is the shear modulus of the steel beam. In the numerical examples presented in section 3, an elastic model is used followed by a yield plateau to reproduce the axial behaviour of the interaction node.

2.6 Reinforcement/particle interaction model

The interaction between the spherical particles representing the concrete and the cylindrical elements representing the reinforcements could be carried out using cylinder/spherical particle detection/interaction schemes. To ease the contact detection process and the contact interaction, each cylindrical element, adopted in the discretization of each reinforcement, is discretized with spherical particles along its length. In this way, it is possible to adopt the spherical particle/spherical particle interaction model previously defined. The spherical particles are rigidly associated with the cylindrical element to which they belong. With this type of model, the discretization of a given reinforcement (a function of the number of cylindrical segments adopted) is independent of the discretization adopted for the particle/steel element interaction.

The unit normal of the concrete spherical particle/steel element spherical particle contact is corrected considering the axial direction of the cylindrical element to which the spherical particle representing the steel element belongs. In this way, the roughness associated with discretizing a cylindrical element as a particle model is eliminated, avoiding the appearance of artificial interlocks.

The elastic and strength properties of the reinforcement/particle contacts are defined using the same methodology adopted for the particle/particle contacts. It is also required that a given concrete particle can only interact with a single contact point of a given group of representative elements of the same steel beam. For the concrete particle/steel particle contact a BL contact model similar to the model adopted for concrete particles interactions is adopted.

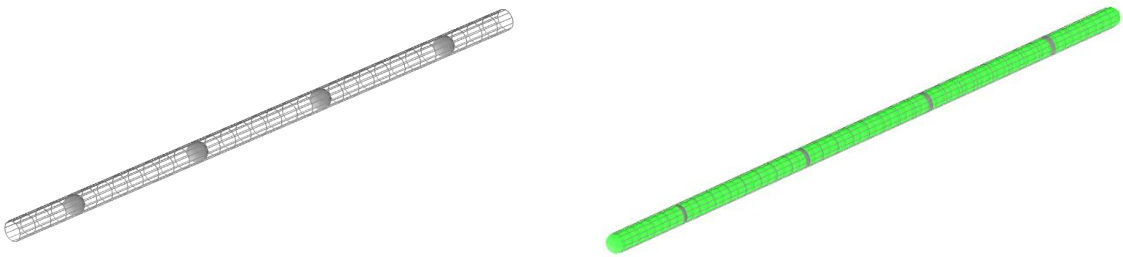

a) 4 cylindrical elements representing steel reinforcement

b) Discretization of each cylindrical element with spherical particles for interaction reasons

Figure 5: Discretization of cylindrical elements with spherical particles.

3 CASE STUDY: THREE POINT BENDING TEST

The PM model was applied to the numerical analysis of experimental bending tests of a three-point beam [23], in which the minimum amount of bending reinforcement in high-strength concrete beams was studied. Three different geometries were considered in the experimental test, in this study only the smallest beam was investigated numerically, Figure 6. The concrete used consists of an aggregate with a maximum size of 12.7 mm in diameter, an average ultimate compressive stress of 91.2 MPa (measured in 160 mm × 160 mm cubic specimens) and a modulus of elasticity of 34.2 GPa, see Table 1. A Poisson's coefficient of 0.15 and a maximum tensile strength of 4.0 MPa was adopted for calibration purposes.

The contact properties, Table 2, were obtained through a simple calibration process, by trial and error, on 160x160x160mm^3 numerical specimens. The elastic contact properties were calibrated, followed by the strength properties adopting uniaxial compression and tensile tests. Due to the computational costs associated with PM models, it was necessary to adopt a particle size higher than the actual concrete particle sizes, thus making it impossible to represent the heterogeneity of the concrete.

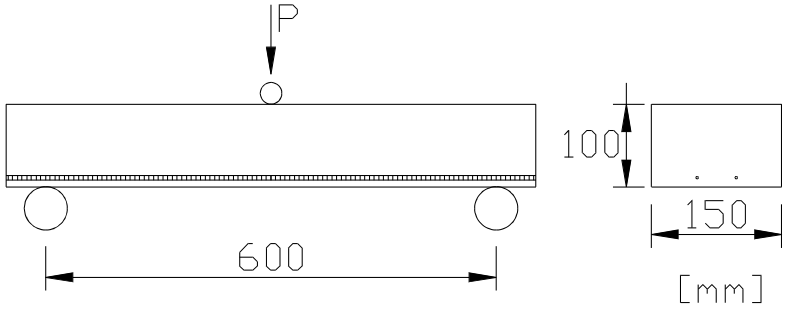

Figure 6: Three point bending test geometry

Table 1: Three point bending test - Elastic and strength BL macroscopic numerical properties

E (GPa)	υ	σ_c (MPa)	σ_t (MPa)
34.2	0.15	91.2	4.0

Figure 7 shows the stress-strain curves and the contact damage evolution obtained in uniaxial compression and uniaxial tensile tests. As shown, it is possible to obtain with a VGCM-3D contact model a compression/tensile maximum stress ratio of approximately 22.

Table 2: Three point bending test - Elastic and strength calibrated VGCM3D contact properties.

$\bar{E}$ (GPa)	α	μ_c	$\sigma_{n.t}$ (MPa)	τ (MPa)	$G_{f.n}$ $[N/m]$	$G_{f.s}$ $[N/mm]$
48.7	0.3	0.50	4.15	21.00	9.002	2380.785

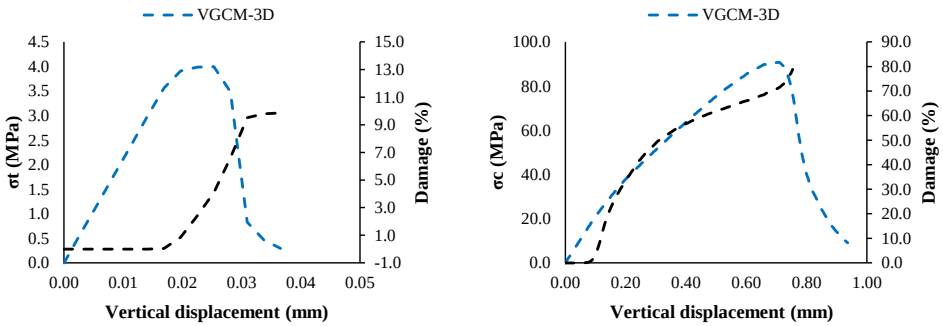

a) Tensile test b) Compression test

Figure 7: Vertical stress-strain curves for uniaxial tensile and compression tests.

Similarly to the experimental tests [23], different steel content and reinforcement bar sizes were considered, as presented in Table 3. Each steel reinforcement bar was discretized with rigid cylindrical elements with a length of 32 mm. A modulus of elasticity of 200.0 GPa was assumed for the reinforcement. Like in the experimental program, the distance of the reinforcement bars from the lower beam edge was equal to one-tenth of the total beam depth. The PM for a 10 mm reinforcement (AN10) has 5987 particles representing the aggregate, 17608 smaller particles representing the cement paste and 260 particles adopted in the discretization of the cylindrical elements representing the reinforcement. The adopted PM models have an average of around 153,165 VGCM-3D contacts.

Table 3 also shows the maximum values of the load obtained in the experimental test [23], and the maximum values predicted with a perfectly elastic interface model of the concrete/reinforcement contact (EL), and with a BL model for the steel/concrete interfaces with contact properties similar to the concrete contact properties (NL-A) and with a BL model for the steel/concrete interface following a 50% reduction of the contact strength properties of the VGCM-3D contact that represents concrete (NL-B). As expected, the elastic contact model has higher maximum ultimate strength load values than those obtained with the BL contact models, in which the predicted maximum strength load values are close to the experimental values, namely when a 50% reduction is adopted (NL-B).

Table 3: Reinforcement properties and corresponding maximum loads.

Experimental	Steel content	Yield limit (MPa)	$P_{Experimental}$ (kN)	$P_{Numerical}$ (EL) (kN)	$P_{Numerical}$ (NL-A) (kN)	$P_{Numerical}$ (NL-B) (kN)
AE 0	0	-	11.8	11.7	-	-
AE 1	1 Φ 4	637	11.9	13.6	11.0	11.0
AE 2	2 Φ 5	569	15.2	26.8	16.4	16.3
AE 3	2 Φ 8	441	27.9	38.9	33,2	30.7
AE 4	2 Φ 10	456	48.7	43.8	39.1	36.0

Figure 8 shows the predicted numerical final deformation, magnified 20 times and Figure 9 presents the predicted final crack patterns, for each steel content and adopted reinforcement bar

size. In all numerical models, cracking initiates at the lower zone of the central part, close to the zone of maximum bending moment. The fractured surface later evolved inwards, towards the area where the vertical load is being applied. For higher reinforcement steel ratios diagonal cracking due to shear loading occurs at later loading stages due to the arc effect from the upper plate in the central zone to the lower supporting plates which is allowed due to the presence of the reinforcement bars.

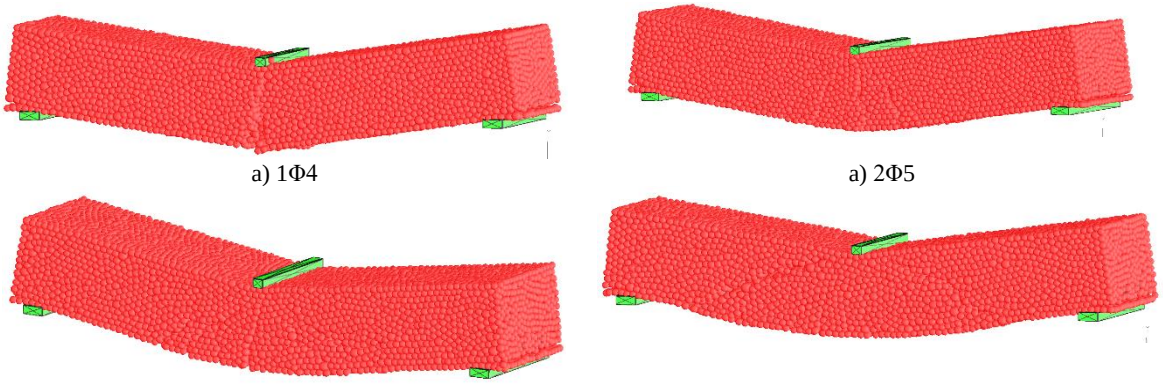

Figure 8: Three point bending test – Amplified deformation.

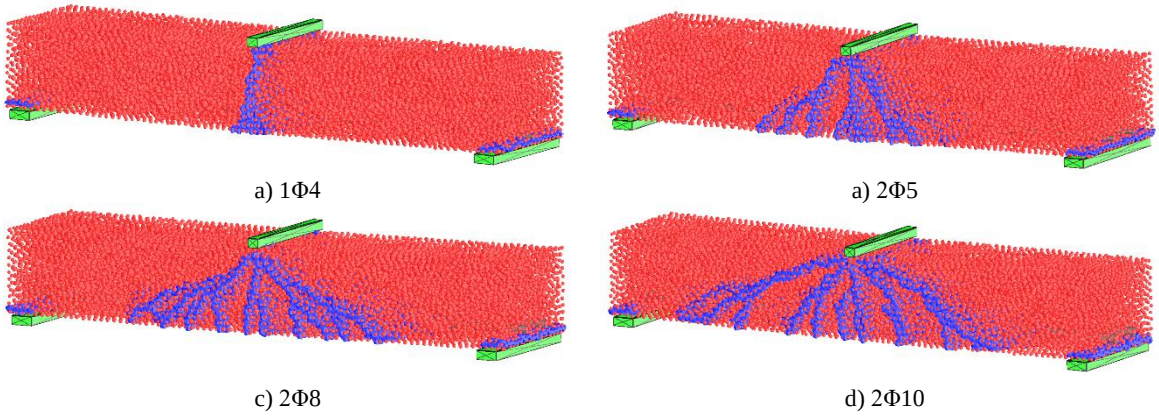

Figure 9: Three point bending test – Final crack patterns.

Figure 10 shows the numerical and experimental load-displacement diagrams for different reinforcement solutions that were evaluated. For the case without reinforcement, the numerical solution shows a good correlation until the peak value is reached, with the numerical response being more brittle than the real one. It would be possible to obtain better performance with a more detailed MP model. In the cases where a BL contact model was adopted for the steel/concrete interaction, there was a much better agreement with the experimental tests, namely when a 50% strength reduction was adopted (NL-B). Figure 10 f) shows that the reinforced PM model can predict the amount of reinforcement for which there is a transition between a ductile and a brittle response. In both the experimental and numerical tests, this

transition occurred for a level of reinforcement corresponding to 2Φ5.

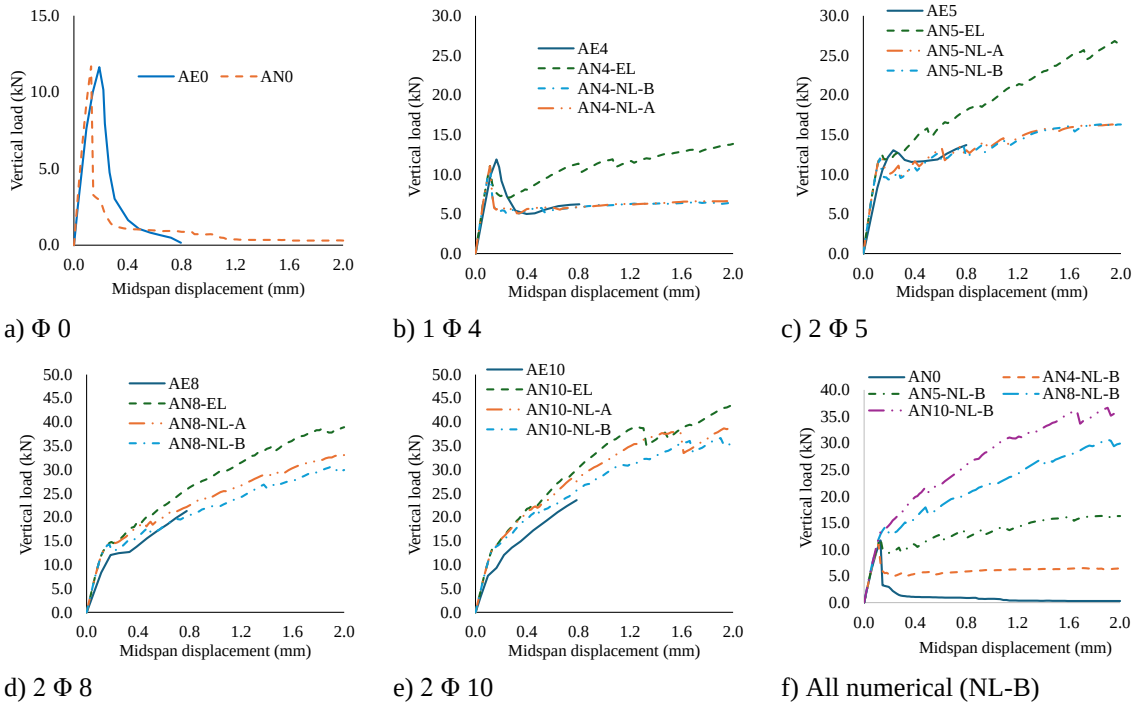

a) Φ 0 b) 1 Φ 4 c) 2 Φ 5

d) 2 Φ 8 e) 2 Φ 10 f) All numerical (NL-B)

Figure 10: Three point Bending test: Load-displacement diagrams (experimental (AE) [23], elastic concrete/reinforcement interface (AN-EL) and BL concrete/reinforcement interfaces for different contact strengths (AN-NL-A and AN-NL-B).

4 CONCLUSIONS

A reinforced PM model is presented which simulates the fracture mechanisms existing in reinforced concrete by considering the aggregate structure, the contact mechanisms and the interaction between the particles and the reinforcement elements modelled with rigid elements of cylindrical geometry, sub-discretized with spherical particles along their length to ease the contact interaction process. The elastic and strength properties of the reinforcement are lumped in the connection zones between cylindrical elements.

As shown, it is possible to calibrate the contact properties of the model in simple tests (uniaxial compression and uniaxial tension), obtaining for different steel contents responses close to those observed experimentally. For a three-point bending test, the reinforced PM model adequately simulates the load-displacement relationship, the maximum load value and the fracture process for different levels of reinforcement. The PM model is shown to predict the transition from a brittle response to a ductile response as the amount of reinforcement increases.

ACKNOWLEDGMENTS

The study presented here is part of the research project StepDam: A step forward for the ability to anticipate and prevent failures of concrete dam foundations, supported by LNEC. The authors would also like to thank the Portuguese Foundation for Science and Technology (FCT)

for funding the Project “Seismic and Structural Health Monitoring for Large Concrete Dams (SSHM4Dams)”, PTDC/ECI-EGC/5332/2020.

REFERENCES

[1] Potyondy, D. and Cundall, P. 2004 “A bonded-particle model for rock.” Int. J. Rock Mech. Min. 41(8): 1329-1364. https://doi.org/10.1016/j.ijrmms.2004.09.011.

[2] Scholtès, L., Donzé, F. 2013. “A DEM model for soft and hard rocks: Role of grain interlocking on strength.” J. Mech. Phys. Solids, 61(2), 352–369. https://doi.org/10.1016/j.jmps.2012.10.005.

[3] Hentz, S., Daudeville, L., Donzé, V. 2004. “Identification and validation of a discrete element model for concrete.” J. Eng. Mech., 130(6), 709–719. https://doi.org/10.1061/(ASCE)0733-9399(2004)130:6(709).

[4] Monteiro Azevedo, N., Lemos, J.V. 2006. “Aggregate shape influence in the fracture behaviour of concrete.” Struct. Eng. Mech. 24(4): 411-427. https://doi.org/10.12989/sem.2006.24.4.411.

[5] Suchorzewski, J., Tejchman, J., Nitka, M. 2018. “Discrete element method simulations of fracture in concrete under uniaxial compression based on its real internal structure.” Int. J. Damage Mech, 27, 578–607. https://doi.org/10.1177/1056789517690915.

[6] Hentz, S., Daudeville, L., Donzé, F. 2009. “Discrete element modeling of a reinforced concrete structure.” J. Mech. Behav. Mater., 19, 249–258. https://doi.org/10.1515/JMBM.2009.19.4.249.

[7] Monteiro Azevedo, N, Lemos, JV, Almeida J. 2010. “A discrete particle model for reinforced concrete fracture analysis”. Struct. Eng. Mech. (2010) 36 (3): 343-361. https://doi.org/10.12989/sem.2010.36.3.343.

[8] Thavalingam, A., Bicanic, N., Robinson, J.I., Ponniah, D.A. 2001. “Computational framework for discontinuous modelling of masonry arch bridges.” Comput. Struct., 79, 1821–1830. https://doi.org/10.1016/S0045-7949(01)00102-X.

[9] Monteiro Azevedo, N., Pinho, F.F.S., Cismaşiu, I., Souza, M. 2022. “Prediction of rubble-stone masonry walls response under axial Compression Using 2D Particle Modelling.” Buildings, 12(8), 1283. https://doi.org/10.3390/buildings12081283.

[10] Peng, Y., Xu, Y.-R., Zhang, X.-F., Meng, H.-L., Lu, X.-Y. 2023. “Investigation on the effects of asphalt mixes and their combinations on asphalt mix shear strength by 3D discrete element method.” Int. J. Pavement Eng. 24(1), 2251078. https://doi.org/10.1080/10298436.2023.2251078.

[11] Câmara, G., Monteiro Azevedo, N., Micaelo, R., Silva, H. 2023. “Generalised Kelvin contact models for DEM modelling of asphalt mixtures.” International Journal of Pavement Engineering, 24(1), 1-15. https://doi.org/10.1080/10298436.2023.2179625.

[12] ASCE Committee on Concrete and Masonry structures. 1981. Finite element analysis of reinforced concrete, Task Committee on Finite Element Analysis of Reinforced Concrete Structures of the Structural Division Committee on Concrete and Masonry Structures, ASCE Special Publication.

[13] Yamamoto Y, Nakamura H, Kuroda I, Furuya N. 2013. Simulation of crack propagation in RC shear wall using a 3D Rigid-Body-Spring model with random geometry. In:

Proceedings of the 8th International Conference on Fracture Mechanics of Concrete and Concrete Structures, Toledo, Spain.

[14] Ogura H, Kunieda M, Nakamura H. 2019. "Tensile fracture analysis of fiber reinforced cement-based composites with rebar focusing on the contribution of bridging forces." J Adv Concr Technol,17(5), 216–31. http://dx.doi.org/10.3151/jact.17.5.216.

[15] Marcon M, Vorel J, Ninčević K, Wan-Wendner R. 2017. "Modeling adhesive anchors in a discrete element framework." Materials,10(8). https://doi.org/10.3390/ma10080917.

[16] Alnaggar M, Pelessone D, Cusatis G. 2019. "Lattice Discrete Particle Modeling of reinforced concrete flexural behavior." J. Struct. Eng.,145(1):04018231. https://doi.org/10.1061/(ASCE)ST.1943-541X.0002230.

[17] Eddy L, Nagai K. 2016. "Numerical simulation of beam-column knee joints with mechanical anchorages by 3D rigid body spring model." Eng. Struct.,126:547–58. https://doi.org/10.1016/j.engstruct.2016.07.054.

[18] Jiradilok P, Nagai K, Matsumoto K. 2019. "Meso-scale modeling of non-uniformly corroded reinforced concrete using 3D discrete analysis." Eng. Struct.,197:109378. https://doi.org/10.1016/j.engstruct.2019.109378.

[19] Cismaşiu, I., Azevedo, N.M., Pinho, F.F.S. 2023. Numerical evaluation of transverse steel connector strengthening effect on the behavior of rubble stone masonry walls under compression using a particle model. Buildings. 13, 987. https://doi.org/10.3390/buildings13040987.

[20] Candeias, M., Monteiro Azevedo, N., Farinha, L. 2018. "A 3D particle model for rock fracture based on the Voronoi diagrams of the granular structure." Geotecnia, 143:171-197 (in Portuguese). https://doi.org/10.24849/j.geot.2018.143.08.

[21] Azevedo, N.M., Farinha, M.L.B., Oliveira, S. 2024. "Assessment of contact laws accounting for softening in 3D rigid concrete particle models." Buildings. 14, 801. https://doi.org/10.3390/buildings14030801.

[22] Kaschube, J. and Dinkler, D. 2021. "A discrete element model for reinforced concrete." Proc. Appl. Math. Mech., 20: e202000258. https://doi.org/10.1002/pamm.202000258.

[23] Bosco C., Carpinteri, A., Debernardi, P.G. 1990. "Minimum reinforcement in high strength concrete." J. Struct. Eng., 116 (2), 427-437. http://doi.org/10.1061/(ASCE)0733-9445(1990)116:2(427).